

1 Projection of changes in tropical cyclone activity and cloud height due
2 to greenhouse warming: global cloud-system-resolving approach
3

4 Yohei Yamada^{1*}, Kazuyoshi Oouchi¹, Masaki Satoh^{1,2},
5 Hirofumi Tomita¹ and Wataru Yanase³
6

7
8 1 *Research Institute for Global Change, Japan Agency for Marine-Earth*
9 *Science and Technology, 3173-25 Showamachi, Kanazawa-ku, Yokohama-Shi,*
10 *Kanagawa 236-0001, Japan*

11 2 *Center for Climate System Research, the University of Tokyo, 5-1-5 Kashiwanoha,*
12 *Kashiwa-Shi, Chiba 277-8568, Japan*

13 3 *Ocean Research Institute, the University of Tokyo, 1-15-1 Minamidai, Nakano-ku,*
14 *Tokyo 164-8639, Japan*
15

16
17 February, 2010
18

.....19 *******Geophysical Research Letters**
20
21
22

23 *Corresponding author: Mr. Yohei Yamada, Research Institute for Global Change, Japan
24 Agency for Marine-Earth Science and Technology, 3173-25 Showamachi, Kanazawa-ku,
25 Yokohama, Kanagawa, 236-0001, Japan (yoheiy@jamstec.go.jp)
26
27
28

29 **Abstract**

30 Tropical cyclone (TC) activity change due to global warming (GW) has been investigated
31 using general circulation models. However, they involve uncertainty in treating the
32 ensemble effects of deep convections. Here we sidestep such uncertainty by using a
33 global cloud-system-resolving model (GCRM) and assess TC changes with a time-slice
34 experiment for the present-day and future GW experiments spanning 5 months each. The
35 results support the Intergovernmental Panel on Climate Change Fourth Assessment
36 Report; reduction in global frequency but increase in more intense TCs. Consistent with
37 recent studies, frequency is reduced over the North Atlantic due to intensified vertical
38 wind shear. Over the Pacific, frequency is almost unchanged and the genesis location
39 shifts eastward under the prescribed El-Niño like sea surface temperature change. With
40 the GCRM's advantage of representing mesoscale properties, we find that the cloud
41 height becomes taller for more intense TCs and that this relationship is strengthened with
42 GW.

43 **1. Introduction**

44 Model projection of the change of tropical cyclone (TC) activity due to global
45 warming (GW) remains a challenging problem. A major problem in the approach with
46 general circulation models (GCMs) comes from uncertainty in the cumulus

47 parameterizations used in the hydrostatic framework [Oouchi et al., 2006]. GCMs are
48 incapable of simulating TCs of realistic intensity under the present-day climate condition
49 [IPCC, 2007]. This is true even for 20-km-mesh atmospheric GCMs (AGCMs), which are
50 among the highest resolution models available [Oouchi et al., 2006]. Significant
51 underestimates of TC intensity over the globe and of frequency over the northwestern
52 Pacific have been found, which are ascribed to some shortcoming in the cumulus
53 parameterization used. In addition, little consensus among models has been found in the
54 projection of regional TC frequency under greenhouse-warmed conditions. As a reason
55 for this, Sugi et al, [2009] suggests that “the regional tropical cyclone frequency change is
56 sensitive to relative SST change distribution”. Reconciling and clarifying all the model
57 uncertainties involves great effort under unified guidance, such as in the Tropical Cyclone
58 Climate Model Intercomparison Project (TC-MIP) [K. Walsh, personal communication,
59 2009].

60 This study is a first attempt to use a GCRM to provide insight into the problem of
61 TC change under a GW climate. An advantage of a GCRM is that it provides a
62 straightforward approach for treating cloud and convection and their interactions with
63 larger-scale disturbances [Satoh et al., 2008], and therefore the uncertainty in the use of
64 cumulus parameterization can be avoided. The aim of this paper is to demonstrate the

65 general performance of GCRM and discuss the potential feasibility of their use to
66 investigate problems related to GW and future TC change.

67 The Nonhydrostatic ICosahedral Atmospheric Model (NICAM) [Satoh et al.,
68 2008], a prototype GCRM, has exhibited great promise in reproducing cloud-associated
69 disturbances in a series of case studies on Madden–Julian oscillation (MJO) [Miura et al.
70 2007a] and TCs [Fudeyasu et al., 2008; Oouchi et al., 2009a]. In addition, the model has
71 successfully captured monsoon-related intraseasonal disturbances [Oouchi et al., 2009b].
72 The success of NICAM in simulating various tropical cloud systems forms the basis of
73 this type of TC projection study. The GW experiment is a timely step to assess NICAM’s
74 potential for next-generation climate modeling [Satoh et al., 2008; Shukla et al., 2009]
75 and is expected to spur further projection and impact studies of future extreme events.

76 **2. Experimental Design**

77 The model configuration of NICAM is the same as that used by Oouchi et al.
78 [2009a]. The mesh interval is approximately 14 km. Although this resolution is coarser
79 than that used in cloud-system-resolving models, it is acceptable for the present purpose
80 because it can capture the large-scale organization of the cloud systems of MJO, TCs, and
81 mesoscale convective features such as the diurnal cycle of precipitation [Miura et al.,
82 2007a, 2007b; Oouchi et al., 2009a; Sato et al., 2009].

83 The experiment follows a time-slice approach [Bengtsson et al., 1996]
84 consisting of a control (CTL) experiment from June to October 2004 and a future GW
85 experiment from May to October at the end of the 21st century. May for GW is regarded as
86 a spin-up period and excluded from the analysis. We chose 2004 as the sample year for
87 the present-day experiment because that year had above-normal global TC activity and a
88 large number of TCs made landfall in Japan. The large computational demand of the
89 GCRM approach prohibits our integrating the model for many months to obtain
90 interannual variability. However, our purpose in this study is not to produce sufficient
91 statistics, but rather to understand the mechanism of TC change associated with GW.

92 For CTL, the boundary conditions of sea surface temperature (SST) and sea ice
93 concentration (SIC) are the same as those in the boreal summer 2004 experiment of
94 Oouchi et al. [2009a]. The conditions for GW are created using the dataset of the World
95 Climate Research Program (WCRP) Coupled Model Inter-comparison Project phase 3
96 (CMIP3) with the method of Mizuta et al. [2008]. The climate forcing for GW is created
97 by adding the SST and SIC differences between the present-day (1979–2003) and GW
98 (2075–2099) periods to the CTL (Fig. 1d). As Yokoi and Takayabu,[2009] said, Fig. 1
99 shows that the SST differences in GW is El-Niño like SST pattern.

100 The carbon dioxide concentration in GW is uniformly twice that in CTL,

101 following scenario A1B of the IPCC's Special Report on Emissions Scenarios (SRES).
102 The initial conditions for GW are taken from a present-day National Centers for
103 Environmental Prediction (NCEP) reanalysis dataset for 0:00 UTC 1 May 2004. The
104 model TCs are tracked using the methodology described by Sugi et al. [2002] and Oouchi
105 et al. [2006]. We compare the simulated TCs with an observational TC dataset (OBS)
106 provided by the Unisys Corporation (<http://weather.unisys.com/hurricane/>). We use 17.5
107 ms^{-1} as the wind speed threshold for TC definition; no artificial tuning of thresholds is
108 required for the 14-km mesh simulation [Walsh et al., 2007].

110 **3. Results**

111 The tracks for CTL are generally consistent with those in OBS (Fig. 1a and 1b).
112 We do not find the deficiency over the northwestern Pacific suggested by Oouchi et al.
113 [2006]. Figure 1c shows that TC tracks shift eastward over the western Pacific (WP) and
114 quiescent over the Atlantic ocean (AO).

115 Table 1 summarizes the TC frequency for OBS, CTL, and GW. The global
116 number (52) for CTL is very close to the observed number of 51. This shows that our
117 14-km mesh simulation realistically reproduces the total TC number without artificial
118 tuning of the threshold for TC definition. In terms of future change, the global frequency

119 is reduced from 52 to 34 (about 40%), but the change depends on the ocean basin.
120 Frequency is decreased over the Indian ocean and AO, whereas it remains almost
121 unchanged over WP and eastern Pacific (EP). Table 1 also shows the sensitivity of the
122 TC numbers to the threshold values of wind speed. This suggests the robustness of the
123 reduction in TC number for GW, which holds even when the other thresholds are
124 changed. In addition, Tab. 1 shows ACE index [Bell and Chelliah, 2006] and TC life
125 time. We find that each TC generated over the WP develops in GW more than that in
126 CTL. Over WP, although life-time and frequency are almost unchanged in both cases,
127 ACE index in GW is larger than that in CTL.

128 We explore the large-scale environmental condition for TC genesis, using the
129 Genesis Potential Index (GPI) proposed by Emanuel and Nolan [2004] and Camargo et al.
130 [2007]. Figure 2 shows the GPI (a, b), the difference between GW and CTL (GW – CTL;
131 c), and the contribution of each constituent term to the entire change (d–g). The relative
132 contribution is assessed by taking the difference (GW – CTL) for only one of the
133 contributing factors with the other factors set to CTL values. The western to central
134 Pacific is marked by an eastward shift of high potential area. In the North Atlantic, a
135 dipole feature of the negative and positive GPI difference (Fig. 2c) is evident. In the
136 negative GPI area, the vertical wind shear, which is unfavorable for TC genesis,

137 dominates the change in other factors. The dipole feature and its association with the
138 reduction trend of Atlantic hurricanes are due to El-Niño like SST forcing [Vecchi and
139 Soden, 2007]. For the western Pacific, the GPI change is explained by change in relative
140 humidity and vertical shear, which closely linked to the specified SST pattern of GW.

141 To investigate the change in intensity, histograms of the maximum wind speed
142 and the minimum sea level pressure (MSP) are displayed in Fig. 3. Overall, TCs of
143 intense class increase; the MSP of the most intense TC is decreased from 902 hPa to 871
144 hPa. Because our 14-km-mesh simulation reproduces realistic wind speeds and MSP of
145 TCs, this result implies that such strong TCs with surface pressure of approximately 870
146 hPa might occur frequently in the future. The trend of intensity increase is statistically
147 significant at the 90 % and 95 % confidence level for wind speed and MSP, respectively,
148 with the Welch's two-sided Student's t-test [Welch, 1947]

149 One of the advantages of the GCRM approach is that mesoscale cloud properties
150 can be discussed using the model results. Figure 4 plots the relationships between MSP
151 and explicitly simulated cloud top height for all the TCs at their most intense stages.
152 Evidently, more intense TCs have higher cloud height, and for the TCs within a similar
153 intensity range, the height is taller in GW than in CTL (the slope of the best-fit regression
154 line is steeper for GW). The tendency is statistically significant at the 99.9 % confidence

155 level with the Welch's two-sided Student's t-test [Welch, 1947]. This finding supports the
156 change in the warm-core structure of hurricanes simulated in a regional hurricane model
157 experiment [Knutson and Tuleya, 1999]. Our results are also consistent with the Carnot
158 heat engine framework conceptualized by Emanuel [1986], in which the potential
159 intensity of TCs is expected to increase under global warming conditions due to
160 increasing SSTs and boundary layer moisture (warm source). In this simple framework,
161 the cold sink associated with and felt by the TC outflow is another factor controlling the
162 thermal efficiency of TCs to a first-order approximation. As the atmosphere is more
163 stabilized in GW, the thermodynamic efficiency is smaller in GW. However, if TCs
164 become taller, their thermodynamic efficiency can increase, and their intensities can be
165 stronger than those in CTL. In fact, the average of the thermal efficiency of the mature
166 stages of TCs is 0.27 for GW and 0.26 for the present climate.

167 **4. Concluding remarks**

168 This paper introduces a new strategy of using a GCRM to investigate changes in
169 TCs under future GW climate conditions. The simulated TC changes are consistent with
170 findings of the IPCC-AR4 report [IPCC, 2007] in terms of a global reduction of
171 frequency and global increase of more intense TCs. It is important to note that the
172 underlying physical implications might be different; the GCRM is capable of tracking the

173 majority of convection-coupled seed vortices that can develop into TCs, and these
174 processes are inadequately represented in GCMs due to uncertainty in cumulus
175 convection schemes [Oouchi et al., 2009a].

176 The aim of the paper is to clarify the mechanism of the projected change in TCs,
177 rather than to obtain statistical robustness of TC characteristics, for which the time
178 integration for 5 months is too short. Our results show that the TC frequency is reduced in
179 AO and that this is explained by intensified vertical shear in the subtropics. In WP, the
180 present-day simulation obtains a TC number very close to the observation; this is a
181 notable result of the GCRM, as current GCMs generally have difficulties in realistic TC
182 simulation in WP [Oouchi et al., 2006]. The projected TC number in WP is almost
183 unchanged because the TC genesis is merely shifted eastward due to the prescribed SST
184 change of the El-Niño pattern. This result also suggests that the projected TC change in
185 WP and AO is sensitive to the pattern of future SST. Our next plan is to identify change in
186 triggering disturbances such as MJO and easterly and equatorial waves, a subject that
187 remains untouched by GCM studies. This investigation will highlight the merits of the
188 GCRM and should provide new insights into issues of GW and TCs.

189

190 **Acknowledgments**

191 The numerical experiments were performed on the Earth Simulator of JAMSTEC under
192 the framework of KAKUSHIN project funded by the Ministry of Education, Culture,
193 Sports, Science and Technology (MEXT), Japan. The Climate Model Intercomparison
194 Project 3 (CMIP3) SST and SIC dataset was provided by Drs. Mizuta, Adachi, and Kitoh
195 (Meteorological Research Institute). The authors thank Drs. Nasuno, Iga, A.T. Noda,
196 Taniguchi, Kodama, Tsushima, A. Noda, Sugi, Matsuno and anonymous reviewers for
197 valuable comments.

200 **References**

- 201 Bengtsson, L., M. Botzet, and M. Esch (1996), Will greenhouse-induced warming over
202 the next 50 years lead to higher frequency and greater intensity of hurricanes?
203 *Tellus*, **48A**, 57–73.
- 204 Bell, G. D., and M., Chelliah (2006), Leading tropical modes associated with interannual
205 and multidecadal fluctuations in North Atlantic hurricane activity, *J. Climate*, **19**,
206 590–612.
- 207 Camargo, S. J., A. H. Sobel, A. G. Barnston, and K. A. Emanuel (2007), Tropical cyclone
208 genesis potential index in climate models, *Tellus*, **59A**, 428–443.

209 Emanuel, K. (1986), An air-sea interaction theory for tropical cyclone. Part I: steady-state
210 maintenance, *J. Atmos. Sci.*, **43**, 585–604.

211 Emanuel, K. and D. S. Nolan (2004), Tropical cyclone activity and the global climate
212 system, paper presented at the 26th Conference on Hurricanes and Tropical
213 Meteorology, *Am. Meteorol. Soc.*, Miami, FL,

214 Fudeyasu, H., Y. Wang, M. Satoh, T. Nasuno, H. Miura, and W. Yanase (2008), The
215 global cloud-system-resolving model NICAM successfully simulated the life cycles
216 of two real tropical cyclones, *Geophys. Res. Lett.*, **35**, L22808,
217 doi:10.1029/2008GL0360033.

218 IPCC (Intergovernmental Panel on Climate Change) (2007), Climate change, the physical
219 science basis contribution of Working Group I to the Fourth Assessment Report of
220 the Intergovernmental Panel on Climate Change. Chapter 8: Climate models and
221 their evaluation, 8.5.3. Tropical Cyclones, Cambridge Univ. Press, Cambridge, pp.
222 628 (eds. Solomon, S., et al.).

223 Knutson, T. R., and R. E. Tuleya (1999), Increased hurricane intensities with
224 CO₂-induced warming as simulated using GFDL hurricane prediction system,
225 *Climate Dyn.*, **15**, 503–186.

226 Miura, H., M. Satoh, T. Nasuno, A. T. Noda, A.T., and K. Oouchi (2007a), A

227 Madden-Julian Oscillation event simulated using a global cloud-resolving model,
228 *Science*, **318**, 1763–1765.

229 Miura, H., M. Satoh, H. Tomita, T. Nasuno, S. Iga, and A. T. Noda (2007b), A
230 short-duration global cloud-resolving simulation with a realistic land and sea
231 distribution, *Geophys. Res. Lett.*, **34**, L02804, doi:10.1029/2006GL027448.

232 Mizuta, R., Y. Adachi, S. Yukimoto, and S. Kusunoki (2008), Estimation of the future
233 distribution of sea surface temperature and sea ice using the CMIP3 multi-model
234 ensemble mean, *Technical Report of the MPI*, **59**.

235 Oouchi, K., J. Yoshimura, H. Yoshimura, K. Mizuta, S. Kusunoki, and A. Noda (2006),
236 Tropical cyclone climatology in a global-warming climate as simulated in a
237 20-km-mesh global atmospheric model: frequency and intensity analysis, *J. Meteor.*
238 *Soc. Japan*, **84**, 259–276.

239 Oouchi, K., A. T. Noda, M. Satoh, B. Wang, S.-P. Xie, H. G. Takahashi, and T. Yasunari
240 (2009a), Asian summer monsoon simulated by a global cloud system-resolving
241 model: diurnal to intra-seasonal variability, *Geophys. Res. Lett.*, **36**, L11815,
242 doi:10.1029/2009GL038271.

243 Oouchi, K., A. T. Noda, M. Satoh, H. Miura, H. Tomita, T. Nasuno, and S. Iga (2009b), A
244 simulated preconditioning of typhoon genesis controlled by a boreal summer

245 Madden-Julian Oscillation event in a global cloud-system-resolving model, *SOLA*, **5**,
246 065-068, doi:10.2151/sola.2009-017.

247 Sato, T., H. Miura, M. Satoh, Y. N. Takayabu, and Y. Wang (2009), Diurnal cycle of
248 precipitation in the tropics simulated in a global cloud-resolving model, *J. Climate*,
249 in press.

250 Satoh, M., T. Matsuno, H. Tomita, H. Miura, T. Nasuno, and S. Iga (2008),
251 Nonhydrostatic icosahedral atmospheric model (MIKAM) for global cloud
252 resolving simulations, *J. Comp. Phys.*, **227**, 3083–3114.

253 Sekiguchi, M., and T. Nakajima (2008), A k-distribution-based radiation code and its
254 computational optimization for an atmospheric general circulation model, *J.*
255 *Quantitative Spectroscopy & Radiative Transfer*, **109**, 2779–2793.

256 Shukla, J., R. Hagedorn, B. Hoskins, J. Kinter, J. Marotzke, M. Miller, T. Palmer, and J.
257 Slingo (2009), Revolution in climate prediction is both necessary and possible, *Bull.*
258 *Ame. Met. Soc.*, 16–19.

259 Sugi, M., A. Noda, and N. Sato (2002), Influence of global warming on tropical cyclone
260 climatology: an experiment with JMA global climate model, *J. Meteor. Soc. Japan*,
261 **80**, 249–272.

262 Sugi, M., A. Noda, H. Murakami, and J. Yoshimura (2009), A reduction in global tropical

263 cyclone frequency due to global warming, *SOLA*, **5**, 164–167,
264 doi:10.2151/sola.2009-042.

265 Vecchi, G. A., and B. J. Soden (2007), Increased tropical Atlantic wind shear in model
266 projections of global warming, *Geophys. Res. Lett.*, **34**, L08702,
267 doi:10.1029/2006GL028905,2007.

268 Walsh, K. J. E., M. Fiorino, C. W. Landsea, and K. L. McInnes (2007), Objectively
269 determined resolution-dependent threshold criteria for the detection of tropical
270 cyclones in climate models and reanalysis, *J. Climate*, **20**, 2307–2314.

271 Welch, B. L., (1947), The generalization of ‘Student’s’ problem when several different
272 population variances are involved, *Biometrika*, **34**, 28-35.

273 Yokoi, A., and Y. Takayabu (2009), Multi-model projection of global warming impact on
274 tropical cyclone genesis frequency over the western north Pacific, *J. Meteor. Soc.
275 Japan*, **3**, 525-538

276

277 **Figure and Table Captions**

278 **Figure 1.** TC tracks (black) from June to October and SST (color shading) averaged for
279 June to October. (a) tracks-CTL/SST-CTL, (b) Unisys best-track/SST-CTL, (c)
280 tracks-GW/SST-GW, and (d)SST difference (GW – CTL).White contours in (c) are for

281 2.2 and 3.0 K.

282

283 **Figure 2.** The GPI for (a) GW, (b) CTL, and (c) the difference of (a) – (b). GPI was
284 defined by Emanuel and Nolan [2004] as $GPI = |10^5 \text{Vor}|^{3/2} |\text{RH}_{700}/50|^3 |\text{PI}/70|^3 |1 + \text{Vsh}|^{-2}$,
285 where Vor, RH_{700} , Vsh, and PI are the absolute vorticity [s^{-1}], relative humidity [%] at 700
286 hPa, vertical wind shear [ms^{-1}] between 850 and 200 hPa, and potential intensity [ms^{-1}],
287 respectively. Here we regard the term A_1 as the term including Vor. Similarly, A_2 , A_3 , and
288 A_4 are the terms including RH_{700} , PI, and Vsh, respectively. (d), (e), (f), and (g) show the
289 contribution of factors in the GPI to the GPI change (i.e., $\Delta \text{GPI}_3 = A_1 A_2 \Delta A_3 A_4$).

290

291 **Figure 3.** Frequency percentage for CTL (blue) and GW (red) as a function of the
292 maximum wind speed at 10 m (left panel) and minimum surface pressure (right panel).

293

294 **Figure 4.** Scatter plots for the cloud top height and the MSP for the simulated TCs. CTL
295 (blue inverted triangle) and GW (red triangle). The regression line for CTL (blue broken
296 line) and GW (red solid line) is $f(x) = 32.8 - 0.0158x$, and $g(x) = 42.5 - 0.0253x$,
297 respectively, where x denotes MSP [hPa]. The cloud height is defined as the highest
298 altitude below which the sum of the solid hydrometeors (snow, cloud ice, and water

299 contents) exceeds $1.0 \times 10^{-5} \text{ kg kg}^{-1}$ at least for 30 grid points in $10^\circ \times 10^\circ$ box.

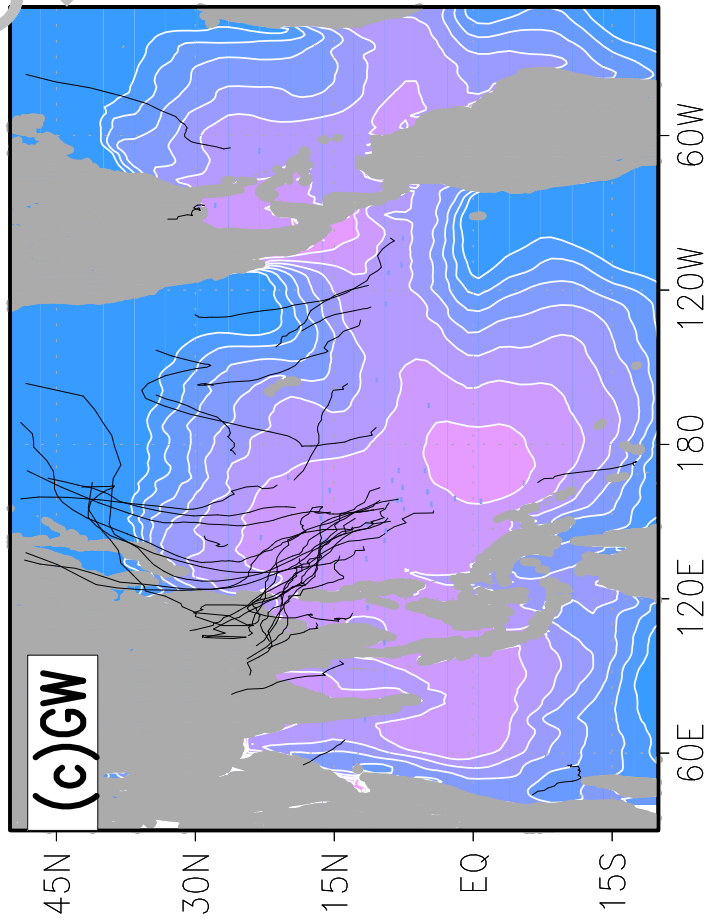
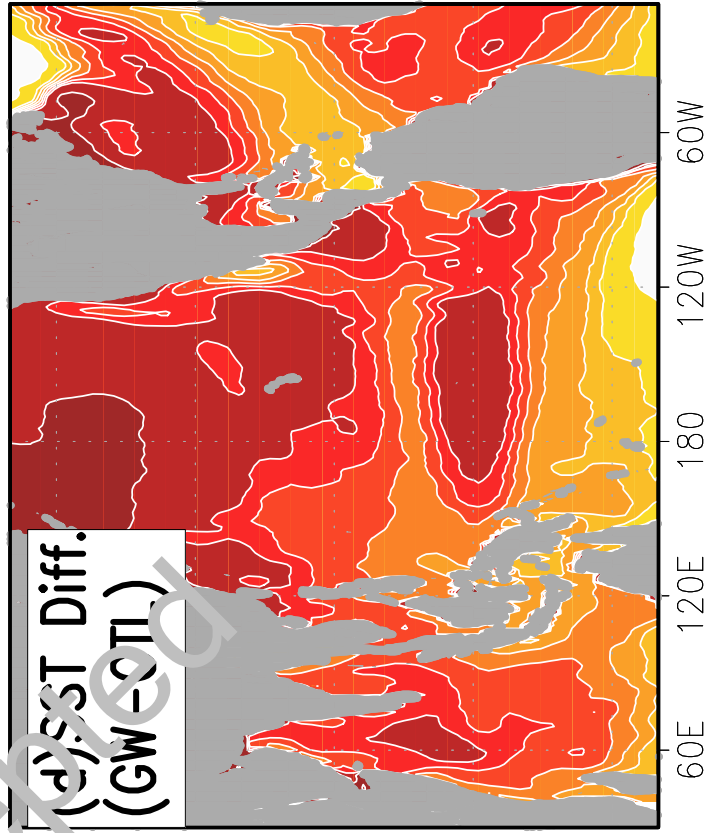
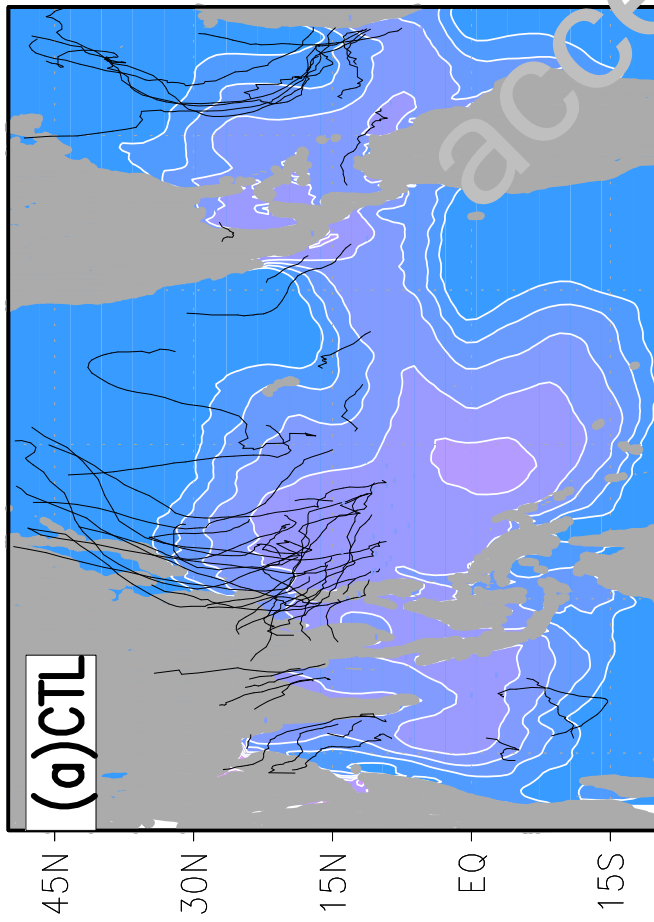
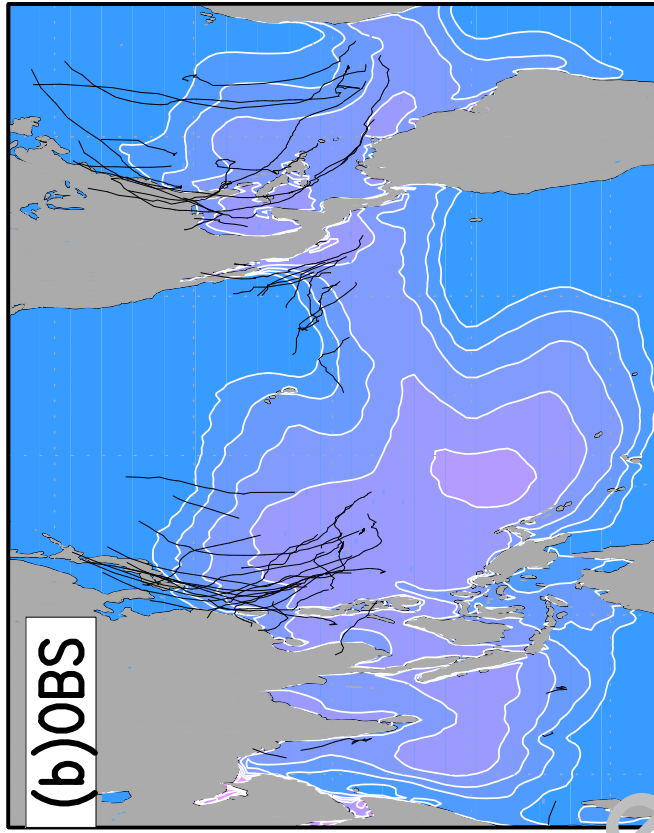
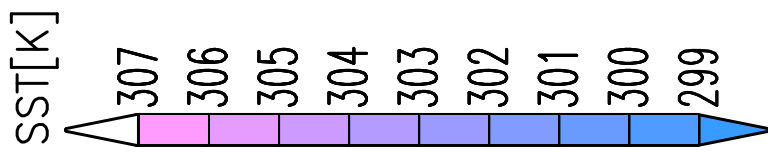
300

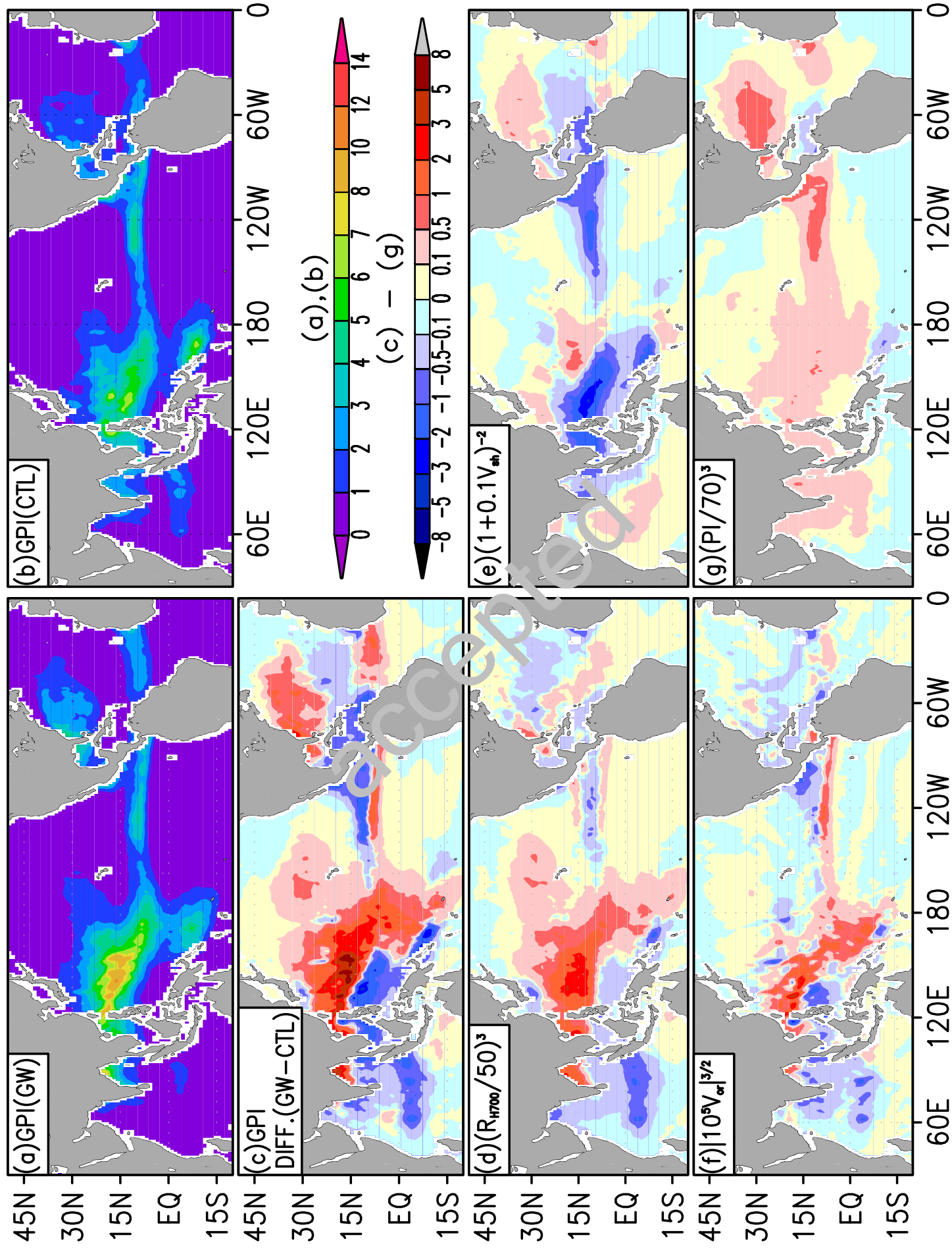
accepted

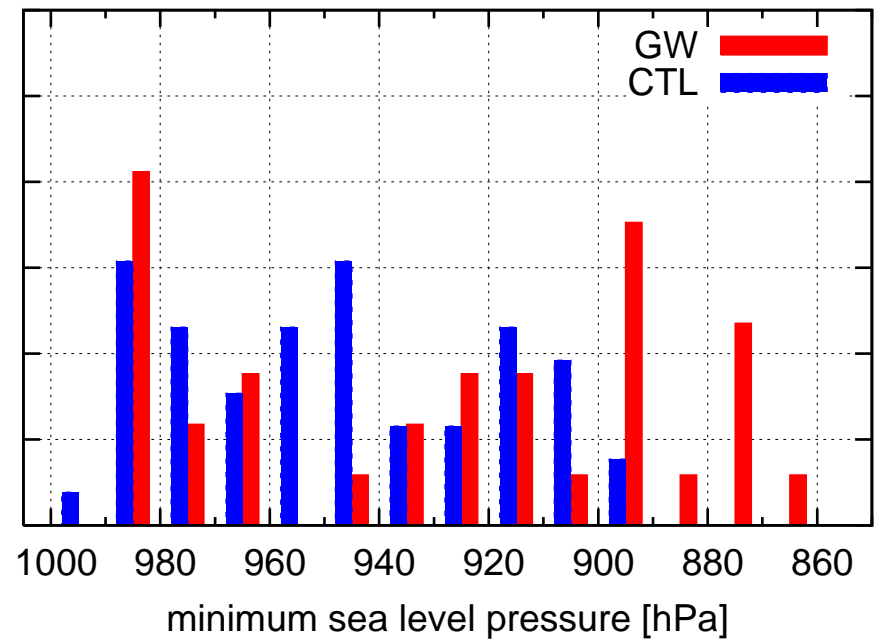
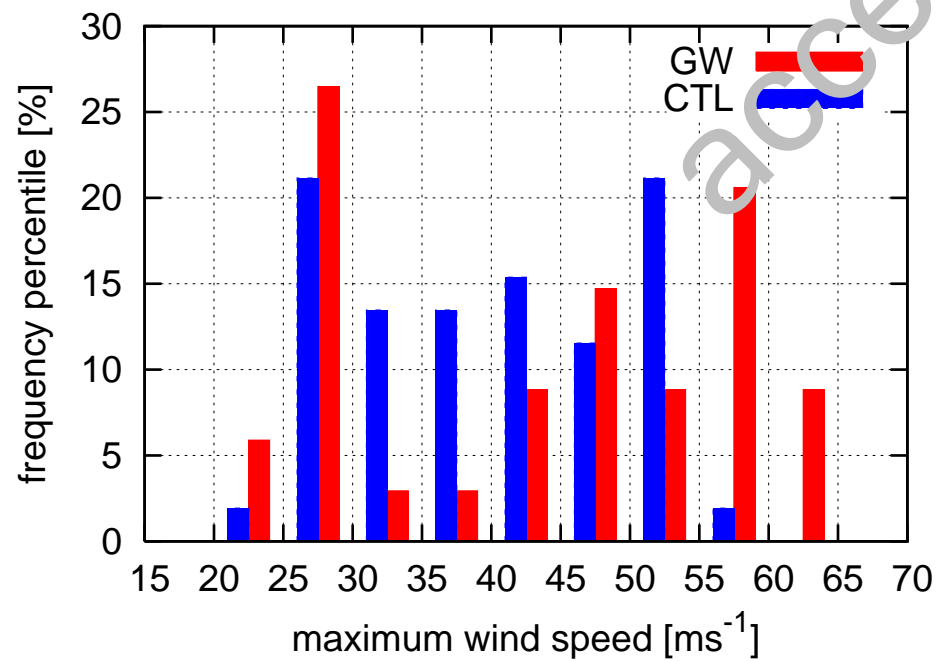
301 **Table 1.** The TC numbers (OBS, CTL, GW) are shown for the globe and each ocean
 302 basin: Indian Ocean (IO; 30°E–100°E); Western Pacific Ocean (WP; 100°E–180); Eastern
 303 Pacific Ocean (EP; 180–90°W); Atlantic Ocean (AO; 90°W–0), when the threshold of
 304 wind speed is 15.5 [ms⁻¹], 17.5 [ms⁻¹] and 20.5 [ms⁻¹], respectively. TC life-time (CTL,
 305 GW) [hours], ACE index (CTL, GW) [× 10⁴ knot²] are also shown.

| | IO | WP | EP | AO | Globe |
|------------------------|------------|------------|------------|-------------|-------------|
| 15.5 (OBS, CTL, GW) | --, 16, 4 | --, 23, 25 | --, 8, 7 | --, 10, 3 | --, 61, 41 |
| 17.5 (OBS, CTL, GW) | 5, 13, 3 | 20, 22, 22 | 12, 7, 7 | 14, 10, 2 | 51, 52, 34 |
| 20.5 (OBS, CTL, GW) | --, 12, 2 | --, 22, 29 | --, 4, 6 | --, 7, 1 | --, 45, 29 |
| TC life-time (CTL, GW) | 79.8, 46.0 | 159, 151 | 78.0, 90.0 | 151.6, 72.0 | 104.6, 89.8 |
| ACE index (CTL, GW) | 49, 7 | 257, 297 | 17, 28 | 78, 9 | 397, 340 |

306







accepted

